Diagn Interv Radiol 2023; DOI: 10.4274/dir.2023.221764

NEURORADIOLOGY

ORIGINAL ARTICLE

Radiomics analysis for predicting malignant cerebral edema in patients undergoing endovascular treatment for acute ischemic stroke

Xuehua Wen
Xingfei Hu
Yanan Xiao
Junfa Chen

PURPOSE

Radiomics analysis is a promising image analysis technique. This study aims to extract a radiomics signature from baseline computed tomography (CT) to predict malignant cerebral edema (MCE) in patients with acute anterior circulation infarction after endovascular treatment (EVT).

METHODS

In this retrospective study, 111 patients underwent EVT for acute ischemic stroke caused by middle cerebral artery (MCA) and/or internal carotid artery occlusion. The participants were randomly divided into two datasets: the training set (n = 77) and the test set (n = 34). The clinico-radiological profiles of all patients were collected, including cranial non-contrast-enhanced CT, CT angiography, and CT perfusion. The MCA territory on non-contrast-enhanced CT images was segmented, and the radiomics features associated with MCE were analyzed. The clinico-radiological parameters related to MCE were also identified. In addition, a routine visual radiological model based on radiological factors and a combined model comprising radiomics features and clinico-radiological factors were constructed to predict MCE.

RESULTS

The areas under the curve (AUCs) of the radiomics signature for predicting MCE were 0.870 ($P < 0.001$) and 0.837 ($P = 0.002$) in the training and test sets, respectively. The AUCs of the routine visual radiological model were 0.808 ($P < 0.001$) and 0.813 ($P = 0.005$) in the training and test sets, respectively. The AUCs of the model combining the radiomics signature and clinico-radiological factors were 0.924 ($P < 0.001$) and 0.879 ($P = 0.001$) in the training and test sets, respectively.

CONCLUSION

A CT image-based radiomics signature is a promising tool for predicting MCE in patients with acute anterior circulation infarction after EVT. For clinicians, it may assist in diagnostic decision-making.

KEYWORDS

Computed tomography, malignant cerebral edema, middle cerebral artery, radiomics, stroke

The safety and efficacy of endovascular treatment (EVT) for anterior circulation large vessel occlusive stroke (LVOS) have been verified in randomized controlled trials. However, nearly 45% of the cases with LVOS cannot recover after EVT.[1,2] Recent evidence has revealed that malignant cerebral edema (MCE) commonly occurs after EVT, and the development of MCE may reduce the benefit–risk ratio of EVT.[3-5] MCE is a severe complication of stroke that occurs in approximately 10% of all patients with stroke. The prognosis for MCE is poor, with a mortality rate of 80% when treated conservatively.[6] Early decompressive surgery effectively lowers mortality and improves the clinical outcomes of patients with MCE.[7] The addition of decompressive craniectomy to the best medical therapy can reduce the mortality rate of MCE by 50%–75%.[8] Hence, the early identification of patients at a high risk of MCE is critical for therapeutic decision-making. The imaging predictors for MCE that have been studied so far primarily involve the characterization of the infarction size, neurovascular condition, and brain perfusion of the patient.[7]

From the Department of Radiology (X.W., Y.X., J.C. ✉cjf2002@126.com), Center for Rehabilitation Medicine, Zhejiang Provincial People's Hospital, Affiliated People's Hospital, Hangzhou Medical College, Zhejiang, China; Department of Radiology (X.H.), The First People's Hospital of Daishan, Zhejiang, China.

Received 10 January 2022; revision requested 16 November 2022; last revision received 24 January 2023; accepted 02 February 2023.

Epub: 17.02.2023

Publication date: xx.xx.2023

DOI: 10.4274/dir.2023.221764

You may cite this article as: Wen X, Hu X, Xiao Y, Chen J. Radiomics analysis for predicting malignant cerebral edema in patients undergoing endovascular treatment for acute ischemic stroke. *Diagn Interv Radiol*. 17 February 2023 DOI: 10.4274/dir.2023.221764 [Epub Ahead of Print].

Diffusion-weighted imaging (DWI) is a valuable technique for identifying the ischemic core. Rapid sequence magnetic resonance imaging (MRI) using DWI and fluid-attenuated inversion recovery sequences has gradually emerged as a new screening modality in people with suspected acute ischemic stroke (AIS), especially where there might be delays in obtaining full sequence brain imaging. However, some limitations still exist, such as limited access at some emergency departments and the contraindications of MRI examination for some patients. Computed tomography (CT) is a commonly used imaging technique in clinical practice for diagnosing and treating AIS. However, some reported prognostic variables (i.e., MCE) are imprecise when using conventional CT methods (i.e., cranial CT scan).[7] Therefore, new approaches that can promptly identify MCE are needed.

Conventional CT images contain information that cannot be evaluated visually but may be assessed using image analysis tools. Image textures correspond to the brightness value and the position of image pixels. Image texture analysis is a quantitative image analysis method that can improve the accuracy of the diagnostic or classification information extracted from different imaging methods, such as ultrasound, CT, and MRI.[9] The correlation between the radiomics signature based on image textures and the progression of MCE after EVT is not fully known. This study hypothesized that the radiomics signature might be an early predictor of MCE in patients with acute anterior circulation infarction after EVT. Furthermore, this study evaluated the predictive potential of a single radiomics signature and a model comprising a radiomics signature as well as clinical factors and routine radiological parameters for MCE.

Methods

This retrospective study was approved by the Zhejiang Provincial People's Hospital's Ethics Committee (approval number: 2020QT038), and informed consent was waived due to its retrospective nature. The clinical data and radiological findings of all subjects were obtained from the medical records and the picture archiving and communication system of our hospital.

Main points

- The development of malignant cerebral edema (MCE) may reduce the benefit–risk ratio of endovascular treatment (EVT).
- Computed tomography-based radiomics analysis may be used to predict MCE.
- A radiomics signature was built to screen patients at high risk of MCE after EVT.

Study population

The clinical and radiological data of patients diagnosed with AIS caused by middle cerebral artery (MCA) and/or internal carotid artery (ICA) occlusion and who had undergone EVT were retrospectively reviewed from the institutional databases between January 2018 and August 2021. Finally, a total of 111 patients were included (Figure 1).

The inclusion criteria were as follows: (1) patients were diagnosed with AIS and underwent EVT; (2) baseline cranial non-contrast-enhanced CT (NCCT), CT angiography (CTA), CT perfusion (CTP) images, and the follow-up CT/MRI images in case of neurological deterioration or within three days after EVT were available; and (3) patients had a causative occlusion of the MCA and/or ICA. The exclusion criteria were as follows: (1) the presence of AIS in the areas supplied by the posterior circulation or bilateral acute ischemic lesions demonstrated by neuroimaging; (2) a modified Rankin Scale score of over two before admission; (3) the presence of symptomatic intracranial hemorrhage; and (4) difficulty in image interpretation due to incomplete images or artifacts.

Endpoint

The primary endpoint was the occurrence of MCE, defined as a midline shift of over 5 mm at the pineal gland or septum pellucidum on the follow-up imaging, with the need for decompressive hemicraniectomy.[3,10-12]

Imaging protocol

All participants underwent baseline CTP and NCCT scans and had follow-up CT or MRI. CTP and NCCT were performed using a 640-slice CT (Aquilion ONE TSX-301A, Toshiba).

The whole-brain NCCT was performed in one rotation (detector width: 16 cm). Moreover, CTP was acquired after the administration of a contrast agent (50 mL; Omnipaque, GE Healthcare) through intravenous (IV) injection at a rate of 6 mL/s, followed by 50 mL of saline (acquisition parameters: scanning width, 5 mm; scanning coverage, 240 mm; 128 mAs; and 120 kV). At 7 s after the

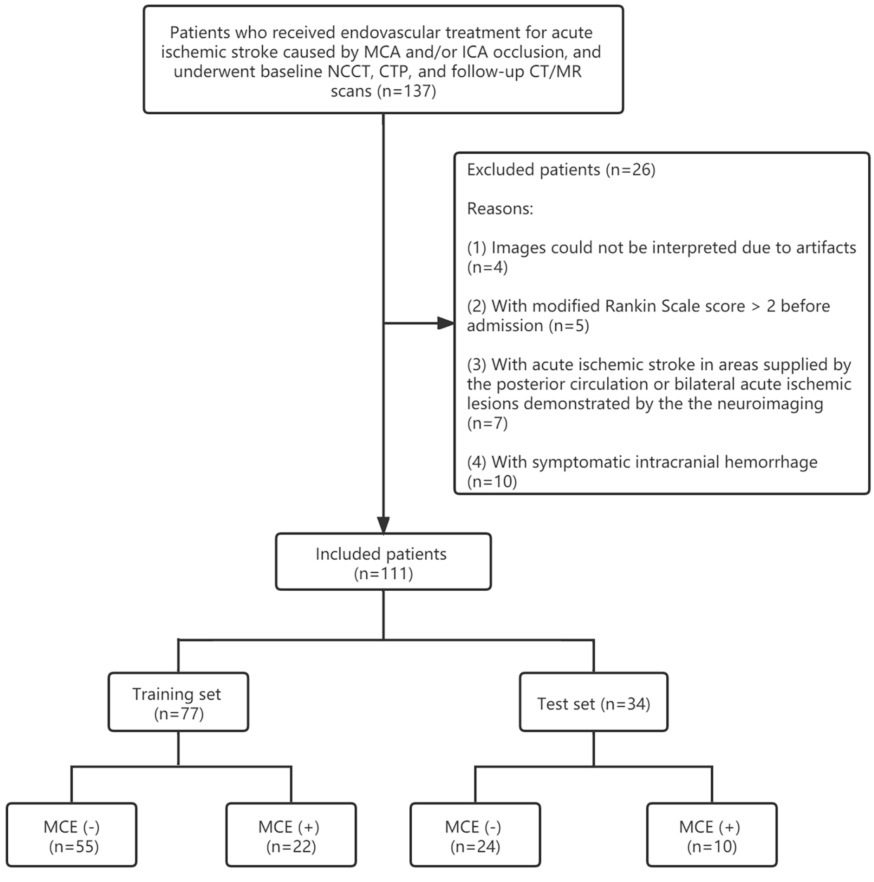

Figure 1. Flowchart of patient enrollment. MCA, middle cerebral artery; ICA, internal carotid artery; NCCT, non-contrast enhanced computed tomography; CTP, computed tomography perfusion; CT, computed tomography; MR, magnetic resonance; MCE, malignant cerebral edema.

injection of the contrast agent, a pulsed full rotation scan was performed with 18 time points acquired over 1 min and a total image acquisition time of 9.5 s. Multiphase CTAs, including venous peak phase, venous late phase, and arterial peak phase images, were generated from CTP images using MIStar (Apollo Medical Imaging Technology).

Clinical and routine radiological assessment

The baseline neurological status of patients at admission was evaluated using the National Institutes of Health Stroke Scale (NIHSS). The recanalization status after EVT was assessed using the modified Thrombolysis in Cerebral Infarction grading system.

Radiological images, including baseline NCCT, CTP, and CTA, as well as follow-up images, were reviewed and evaluated by two neuroradiologists (H and X, with 6 and 10 years of clinical experience, respectively). Any discordant interpretations between the two raters were resolved by consensus through discussion.

The Alberta Stroke Program Early CT Score (ASPECTS) was calculated by subtracting the score of the low-density regions from a total score of 10 on NCCT images.[13]

On CTA images, the thrombosis burden was quantified to assess the clot in the anterior circulation using the clot burden score (CBS), which starts at 10 and is deducted based on the loss of contrast opacification on CTA.[14] The leptomeningeal collateral status was evaluated on a 0–3 scale: 0, absent collateral filling; 1, ≤50% collateral filling; 2, >50% but <100% collateral filling; and 3, ≥100% collateral filling when compared with the non-occluded side.[15]

On CTP images, the ischemic core was defined by a decrease in the relative cerebral blood flow to less than 30% of normal. The ischemic lesion was defined as brain tissues with a delay time (DT) of >3 s based on MIStar.

Image preprocessing and radiomics feature selection

Radiomics analysis was conducted based on baseline cranial NCCT (Figure 2).

Image data preprocessing, including gray-level discretization, intensity normalization, and image interpolation, was carried out using the AK software (version 3.0.0. R, Artificial Intelligence Kit, GE Healthcare).

The region of interest (ROI) of the whole MCA territory was manually segmented on a 3D volume of interest on NCCT images using the ITK-SNAP software (www.itksnap.org). The intra- and inter-rater agreement on the ROI segmentation was evaluated using intraclass correlation coefficients. Rater H segmented the ROIs twice within a 2 month interval. Intra-rater ICC was determined by comparing the two measurements of rater H. Inter-rater ICC was calculated by comparing the ROIs in 30 randomly selected patients (measured by raters X and H).

The extracted features included haralick, histogram, formfactor, gray level co-occurrence matrix, run-length matrix, and gray level size-zone matrix. For each patient, 396 features were extracted, which were then standardized to remove the unit limits of the data. Dimension reduction was carried out using the correlation test, Mann–Whitney U test, and analysis of variance. The features were further selected using the least absolute shrinkage and selection operator (LASSO).

Development of the radiomics signature

Multivariate logistic regression analysis was used to construct the radiomics signature, which was then used to predict MCE based on selected features using the LASSO. Subsequently, the radiomics score (rad-score) of each patient was calculated. The formula was derived from the training set data and was then used to determine the rad-score of the patient in the test set. The predictive efficiency of the radiomics signature was evaluated using the receiver operating characteristic (ROC) curves in both the training and test sets.

Development of the prediction model for malignant cerebral edema

All parameters (i.e., sex, age, history of hypertension, atrial fibrillation, hyperlipidemia, diabetes mellitus, alcohol abuse, smoking, baseline NIHSS, hyperdense vessel sign of the MCA, ASPECTS, collateral score, occlusion site, CBS, ischemic lesion volume, ischemic core volume, IV-type plasminogen activator (tPA), time from onset to groin puncture, reperfusion grade, and the radiomics signature) were screened to identify variables associated with MCE. Furthermore, multivariate regression analysis was performed to construct a prediction model for MCE. The model calibration was assessed using the Hosmer–Lemeshow test. The ROC curve was used to evaluate the predictive ability of the model.

Statistical analysis

The MedCalc v15.2.2, SPSS v21.0, and Microsoft R Open v3.3.1 software were used for statistical analyses. Descriptive statistics were presented as median (first quartile and third quartile) for non-normally distributed variables, and the mean ± standard deviation was used for the normally distributed variables. Categorical variables were report-

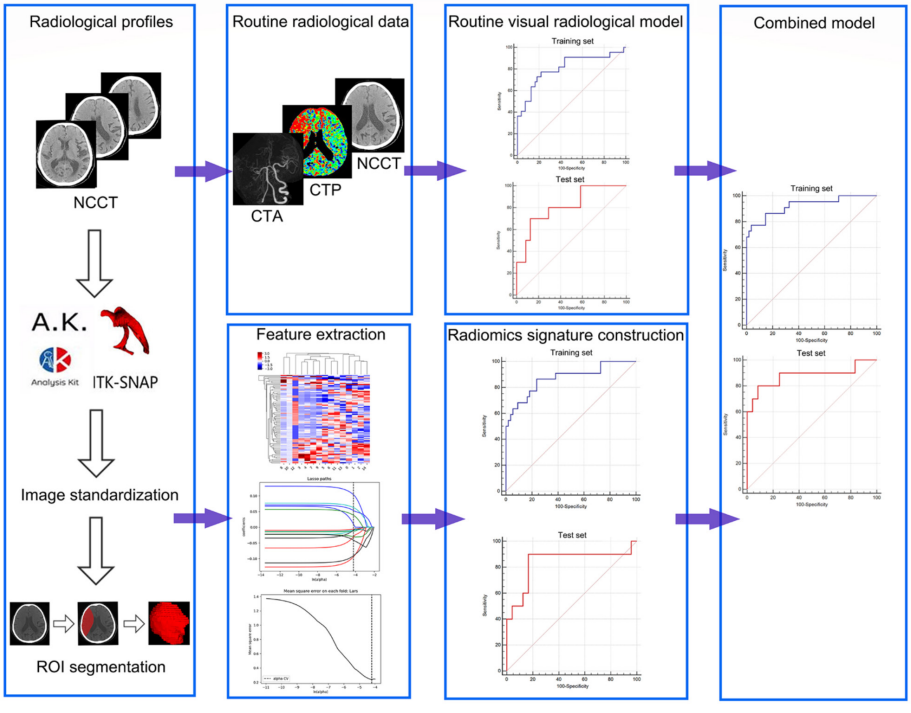

Figure 2. Workflow of radiomics analysis. NCCT, non-contrast enhanced computed tomography; CTA, CT angiography; CTP, CT perfusion; ROI, region of interest.

ed as frequencies (percentages). The LASSO analysis was conducted based on the minimum criterion by 10 fold cross-validation. The Student's t-test, Mann–Whitney U test, Pearson's chi-square test, and Fisher's exact test were used to identify MCE-associated variables. The Youden index in the ROC analysis was used to determine the best cut-off point of CTP parameters and NCCT ASPECTS for identifying patients with MCE. Multivariate regression analysis was performed to establish the radiomics signature, the routine visual radiological model, and the combined model for predicting MCE. The ROC curves were compared using the method developed by DeLong et al.[16] The significance level was established as $\alpha = 0.05$.

Results

The intra- and inter-rater reliability

The intra-rater agreement on the ROI segmentation between the two measurements from the same rater was 0.896 ($P < 0.001$). The inter-rater agreement between the two raters was 0.842 ($P < 0.001$).

Baseline characteristics

A total of 111 patients were randomly split into two datasets at a ratio of 7:3[17] as follows: the training set (n = 77) and the test set (n = 34). There were no significant differences in the clinical or routine radiological characteristics between the two sets (Table 1). The rad-score, ASPECTS, ischemic core volume, DT >3 s lesion volume, and IV-tPA were significantly different between the MCE (+) and MCE (-) groups in the training set (Table 2).

The radiomics signature

After identifying 187 features using the Mann–Whitney U test and analysis of variance, 22 features were retained after the Spearman correlation analysis. Moreover, the LASSO analysis was performed, and 15 features remained (Supplementary Table 1). The rad-score was obtained using the LASSO model, with a linear combination of the 15 features (Supplementary Materials). The values of the 15 features of each subject were placed into the calculation formula, and the rad-score was obtained to indicate the predictive efficiency for MCE.

The sensitivity, specificity, and AUC of the radiomics signature for predicting MCE in the training set were 86.36%, 76.36%, and 0.870 [95% confidence interval (CI): 0.773–0.967], respectively (Figure 3). The radiomics signature showed satisfying goodness-of-fit ($P = 0.361$). The sensitivity, specificity, and AUC in the test set were 90.00%, 83.33%, and 0.837 (95% CI: 0.655-1), respectively (Figure 3).

The routine visual radiological model

The routine radiological parameters for the prediction of MCE were as follows: 1) ASPECTS with an AUC of 0.800 (95% CI, 0.683–0.917; $P < 0.001$); 2) ischemic core volume with an AUC of 0.793 (95% CI, 0.675–0.910; $P < 0.001$); and 3) DT >3 s lesion volume with an AUC of 0.725 (95% CI, 0.580–0.870; $P = 0.002$). The best cut-off values for the ASPECTS, ischemic core volume, and DT >3 s lesion volume were 7, 37, and 235, respectively (Table 3).

The sensitivity, specificity, and AUC of the routine visual radiological model based on the above radiological parameters were 77.27%, 78.18%, and 0.808 (95% CI: 0.687–0.929), respectively, in the training set (Figure 3). The routine visual radiological model showed satisfying goodness-of-fit ($P = 0.200$). The sensitivity, specificity, and AUC in the test set were 70.00%, 87.50%, and 0.813 (95% CI: 0.649–0.976), respectively (Figure 3).

The combined model

The combined model for predicting MCE included the rad-score, ASPECTS, ischemic core volume, DT >3 s lesion volume, and IV-tPA.

In the training set, the sensitivity, specificity, and AUC of the combined model were 77.27%, 96.36%, and 0.924 (95% CI: 0.850–0.998), respectively (Figure 3). The combined model showed satisfying goodness-of-fit ($P = 0.662$). In the test set, the sensitivity, specificity, and AUC were 80.00%, 91.67%, and 0.879 (95% CI: 0.712–1), respectively (Figure 3).

The participants were divided into high- and low-risk groups according to the optimal diagnostic cut-off value of the model (0.390). The number of patients with MCE (+) was significantly different between the high- and low-risk groups in the training set ($P < 0.001$).

Table 1. Characteristics of the training and test sets

Variable	Training set (n = 77)	Test set (n = 34)	*P* value
Male gender, n (%)	49 (63.6%)	22 (64.7%)	0.914
Age (years), mean ± SD	72.1 ± 13.7	70.6 ± 12.7	0.575
Hypertension, n (%)	54 (70.1%)	24 (70.6%)	0.961
Diabetes mellitus, n (%)	11 (14.3%)	5 (14.7%)	1.000
Hyperlipidemia, n (%)	16 (20.8%)	3 (8.8%)	0.123
Atrial fibrillation, n (%)	40 (51.9%)	14 (41.2%)	0.295
Smoking, n (%)	21 (27.3%)	11 (32.4%)	0.586
Alcohol abuse, n (%)	15 (19.5%)	9 (26.5%)	0.410
Baseline NIHSS, median (Q1, Q3)	17 (13–21)	17 (14–20)	0.951
ASPECTS on NCCT, median (Q1, Q3)	8 (5–10)	8 (6–9)	0.748
HVS of MCA, n (%)	43 (55.8%)	14 (41.2%)	0.154
Collateral score, median (Q1, Q3)	1 (1–1)	1 (1–2)	0.054
Vessel occlusion			
Isolated MCA occlusion, n (%)	46 (59.7%)	18 (52.9%)	0.504
Isolated ICA occlusion, n (%)	5 (6.5%)	2 (5.9%)	1.000
Tandem ICA + MCA occlusion, n (%)	26 (33.8%)	14 (41.2%)	0.454
CBS, median (Q1, Q3)	6 (4–6)	5 (4–6)	0.165
Baseline CTP			
Ischemic core volume (mL), median (Q1, Q3)	36 (9–84)	26 (10–63)	0.550
DT >3 s lesion volume (mL), median (Q1, Q3)	144 (85–231)	133 (67–237)	0.916
Treatment characteristics			
IV-tPA, n (%)	26 (33.8%)	7 (20.6%)	0.161
Onset to groin puncture in hours, median (Q1, Q3)	5.1 (3.5–7.6)	5.5 (3.7–7.3)	0.703
mTICI ≥2b, n (%)	72 (93.5%)	30 (88.2%)	0.452

SD, standard deviation; NIHSS, National Institutes of Health Stroke Scale; Q1, first quartile; Q3, third quartile; NCCT, non-contrast-enhanced computed tomography; ASPECTS, Alberta Stroke Program Early CT Score; HVS, hyperdense vessel sign; MCA, middle cerebral artery; ICA, internal carotid artery; CBS, clot burden score; CTP, computed tomography perfusion; DT, delay time; IV-tPA, intravenous-tPA; mTICI, modified thrombolysis in cerebral infarction.

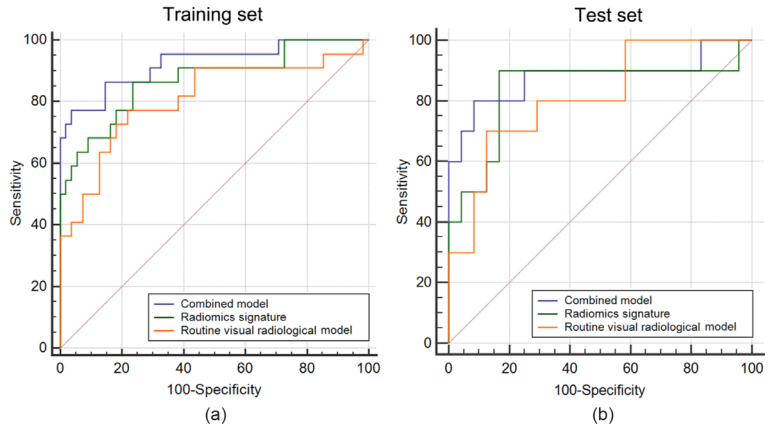

Figure 3. (a) The ROC curve of the radiomics signature [AUC, 0.870 (0.773–0.967)], routine visual radiological model [AUC, 0.808 (0.687–0.929)], and combined model [AUC, 0.924 (0.850–0.998)] for predicting MCE in the training set. **(b)** The ROC curve of the radiomics signature [AUC, 0.837 (0.655–1)], routine visual radiological model [AUC, 0.813 (0.649–0.976)], and combined model [AUC, 0.879 (0.712–1)] for predicting MCE in the test set. ROC, receiver operating characteristic; AUC, area under the curve; MCE, malignant cerebral edema.

Table 2. Comparison between patients with MCE (+) and MCE (-) in the training set

Variable	MCE (n = 22)	non-MCE (n = 55)	*P* value
Male gender, n (%)	15 (68.2%)	34 (61.8%)	0.600
Age (years), mean ± SD	73.0 ± 13.4	71.8 ± 13.9	0.731
Hypertension, n (%)	15 (68.2%)	39 (70.9%)	0.813
Diabetes mellitus, n (%)	3 (13.6%)	8 (14.5%)	1.000
Hyperlipidemia, n (%)	6 (27.3%)	10 (18.2%)	0.371
Atrial fibrillation, n (%)	13 (59.1%)	27 (49.1%)	0.428
Smoking, n (%)	5 (22.7%)	16 (29.1%)	0.571
Alcohol abuse, n (%)	6 (27.3%)	9 (16.4%)	0.342
Baseline NIHSS, median (Q1, Q3)	18 (15–21)	17 (13–22)	0.436
ASPECTS on NCCT, median (Q1, Q3)	5 (3–7)	8 (7–10)	<0.001*
HVS of MCA, n (%)	13 (59.1%)	30 (54.5%)	0.717
Collateral score, median (Q1, Q3)	1 (1–1)	1 (1–1)	0.850
Vessel occlusion			
Isolated MCA occlusion, n (%)	10 (45.5%)	36 (65.5%)	0.106
Isolated ICA occlusion, n (%)	1 (4.6%)	4 (7.3%)	1.000
Tandem ICA + MCA occlusion, n (%)	11 (50%)	15 (27.3%)	0.057
CBS, median (Q1, Q3)	5 (4–6)	6 (4–7)	0.154
Baseline CTP			
Ischemic core volume (mL), median (Q1, Q3)	85 (42–134)	22 (8–55)	<0.001*
DT >3 s lesion volume (mL), median (Q1, Q3)	246 (130–304)	120 (77–192)	0.002*
Treatment characteristics			
IV-tPA, n (%)	2 (9.1%)	24 (43.6%)	0.004*
Onset to groin puncture in hours, median (Q1, Q3)	5.5 (2.9–8.3)	5.0 (3.5–7.5)	0.839
mTICI ≥2b, n (%)	19 (86.4%)	53 (96.4%)	0.137
Rad-score, mean ± SD	3.54 ± 13.62	-2.59 ± 2.10	0.048*

*represents $P < 0.05$. MCE; malignant cerebral edema; SD, standard deviation; NIHSS, National Institutes of Health Stroke Scale; Q1, first quartile; Q3, third quartile; NCCT, non-contrast-enhanced computed tomography; ASPECTS, Alberta Stroke Program Early CT Score; HVS, hyperdense vessel sign; MCA, middle cerebral artery; ICA, internal carotid artery; CBS, clot burden score; CTP, computed tomography perfusion; DT, delay time; IV-tPA, intravenous-tPA; mTICI, modified thrombolysis in cerebral infarction.

Additionally, the results showed that the patients categorized into the high-risk group in the test set were all patients with MCE (+) (Figure 4).

The AUCs of the radiomics signature and the combined model were significantly different ($P = 0.049$). The AUCs of the combined model and the routine visual radiological model were also significantly different ($P = 0.020$). However, there was no significant difference in the AUC between the radiomics signature and the routine visual radiological model ($P = 0.354$) (Table 4).

Discussion

MCE is a life-threatening condition with high mortality rates. It is usually secondary to the acute occlusion of the proximal MCA trunk or the distal ICA.[18] Pathophysiologically, early damage to cerebrovascular autoregulation in the tissues surrounding the infarction, increased vascular permeability, and the loss of the integrity of the endothelial basal layer altogether play important roles in the progression of MCE.[19,20] The early detection of MCE and the use of decompressive surgery can improve the clinical outcomes of patients with MCE.[21,22] However, the current methods for detecting MCE are mainly reactive: waiting for signs of clinical deterioration and mass effect to appear before surgical intervention. Therefore, the identification of early predictors for MCE is of high importance.

Texture feature analysis is widely used in radiomics, which allows the quantification of internal heterogeneity that may not be perceived by the naked eye, thus promoting the identification and classification of different tissues.[23] Until recently, few studies have performed texture analysis of cerebral infarction. CT radiomics based on texture features showed good performance in identifying hyperacute or AIS lesions, assessing the extent of ischemic lesions, and determining the time from symptoms onset in basal ganglia infarction.[24-26] Kuang et al.[27] developed an automated method to compute the ASPECTS on NCCT images from patients with AIS. Additionally, texture analysis based on MRI effectively identified the presence of ischemic stroke lesions and detected hemorrhagic transformation in patients with AIS.[28,29] Furthermore, in patients with stroke, the texture features of brain MRI may provide early markers for poststroke cognitive impairment.[30] The potential of texture features for predicting MCE in patients with AIS caused by MCA and/or ICA occlusion after EVT was evaluated. By constructing a radiomics model, it was found

that the radiomics signature based on texture features was a valuable tool for identifying patients at a high risk of MCE after EVT, with AUCs of 0.870 and 0.837 in the training and test sets, respectively.

By analyzing the correlation between clinico-radiological factors and MCE, it was found that the ASPECTS on NCCT, ischemic core volume, DT >3 s lesion volume, and IV-tPA were correlated with MCE. The ASPECTS, ischemic core volume, and DT >3 s lesion volume can indicate the extent of ischemia or infarct lesion. Compared with patients with MCE (-), patients with MCE (+) showed lower ASPECTS, larger ischemic core volume, and larger DT >3 s lesion volume. This finding suggested that ischemia or infarction core during the early stage was more severe in patients with MCE (+) than in patients with MCE (-), which was consistent with the findings of Tracol et al.[31] A midline shift of over 3.9 mm and an infarct volume of more than 220 mL are predictors of severe brain edema and herniation.[32] This study's results further showed that the proportion of the use of IV-tPA in patients with MCE (+) was lower than that in patients with MCE (-). It suggested that IV-tPA could reduce the incidence of MCE, which was in line with the findings of Fuhrer et al.[33] Treatment with IV-tPA lowered the odds of experiencing MCE, with a reduced odds ratio of 0.88 (95% CI: 0.83–0.94).

With the development of analytical approaches and high-throughput technology, the multiparameter approach has recently become a useful tool for improving diagnostic performance.[34] Therefore, this study built a model combining the radiomics signature, clinical factors, and routine visual radiological factors to predict MCE. Parameters related to MCE, such as the radiomics signature, ASPECTS, ischemic core volume, DT >3 s lesion volume, and use of IV-tPA, were included in this model. The combined model exhibited better differentiation capabilities than the radiomics signature or the routine visual radiological model, with AUCs of 0.924 and 0.879 in the training and test sets, respectively.

The limitations of this study should be noted. First, information and selection biases may exist due to the retrospective nature of this study. Therefore, the validation of the results in a prospective study is required. Second, the sample size was considerably small, and the proposed models were not externally validated. Third, the difference between the combined model and radiomics signature or the routine visual radiological model was small, with only borderline statistical significance between the combined model and radiomics signature. Therefore, a large-scale, multicenter study is required to validate the proposed multimodal diagnostic approach. Despite the abovementioned limitations, a prediction model for MCE after EVT was established in this study by combining the radiomics signature, clinical factors, and routine radiological factors, which may facilitate the accurate early prediction of MCE in patients with acute anterior circulation infarction after EVT.

In conclusion, this study constructed a model for predicting MCE in patients with acute anterior circulation infarction after EVT. These findings may contribute to the accurate and early prediction of MCE and assist clinical decision-making.

Table 3. AUC-ROC analysis of CTP and NCCT ASPECTS cut-off values for patients with MCE (-)

	AUC (95% CI)	*P* value	Best cut-off value	Sensitivity (%)	Specificity (%)
ASPECTS	0.800 ± 0.060 (0.683–0.917)	<0.001*	7	81.82	67.27
Ischemic core volume	0.793 ± 0.060 (0.675–0.910)	<0.001*	37	86.36	67.27
DT >3 s lesion volume	0.725 ± 0.074 (0.580–0.870)	0.002*	235	59.09	90.91

*represents $P < 0.05$. MCE, malignant cerebral edema; AUC, area under the curve; ROC, receiver operating characteristic; NCCT, non-contrast enhanced computed tomography; ASPECTS, Alberta Stroke Program Early CT Score; DT, delay time; CI, confidence interval; CTP, computed tomography perfusion.

Table 4. Comparison of the ROC curves

Variable	Difference between the areas (95% CI)	*P* value
Combined model vs. radiomics signature	0.0537 (0.0001–0.107)	0.049*
Combined model vs. routine visual radiological model	0.1160 (0.0179–0.213)	0.020*
Radiomics signature vs. routine visual radiological model	0.0620 (-0.0691–0.193)	0.354

*represents $P < 0.05$. ROC, receiver operating characteristic; CI, confidence interval.

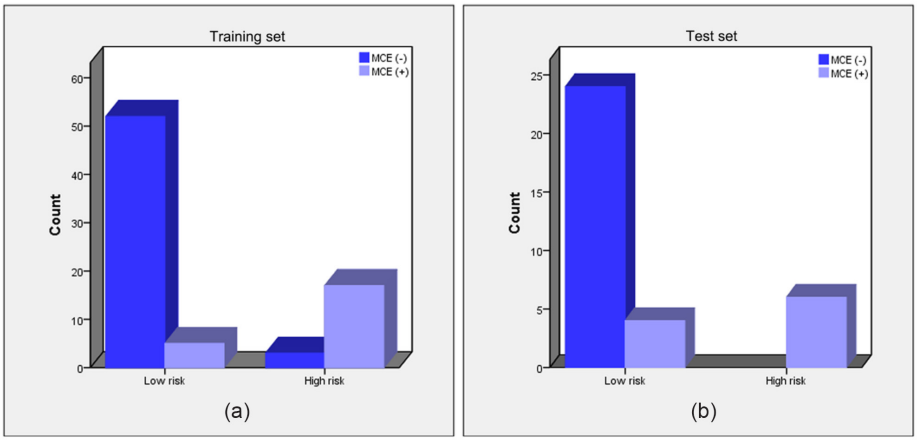

Figure 4. (a, b) Classification performance of the combined model in the training and test sets. MCE, malignant cerebral edema.

Conflict of interest disclosure

The authors declared no conflicts of interest.

Funding

This work was supported by grants-in-aide from the health commission of Zhejiang province (grant number: 2022RC105) and the excellent scientific research foundation of Zhejiang Provincial People's Hospital (grant number: ZRY2021A007).

References

1. Goyal M, Menon BK, van Zwam WH, et al. Endovascular thrombectomy after large-vessel ischaemic stroke: a meta-analysis of individual patient data from five randomised trials. *Lancet*. 2016;387(10029):1723-1731. [CrossRef]

2. Zi W, Wang H, Yang D, et al. Clinical effectiveness and safety outcomes of endovascular treatment for acute anterior circulation ischemic stroke in China. *Cerebrovasc Dis*. 2017;44(5-6):248-258. [CrossRef]
3. Huang X, Yang Q, Shi X, et al. Predictors of malignant brain edema after mechanical thrombectomy for acute ischemic stroke. *J Neurointerv Surg*. 2019;11(10):994-998. [CrossRef]
4. Kimberly WT, Dutra BG, Boers AMM, et al. Association of reperfusion with brain edema in patients with acute ischemic stroke: a secondary analysis of the MR CLEAN trial. *JAMA Neurol*. 2018;75(4):453-461. [CrossRef]
5. Davoli A, Motta C, Koch G, et al. Pretreatment predictors of malignant evolution in patients with ischemic stroke undergoing mechanical thrombectomy. *J Neurointerv Surg*. 2018;10(4):340-344. [CrossRef]
6. Oppenheim C, Samson Y, Manaï R, et al. Prediction of malignant middle cerebral artery infarction by diffusion-weighted imaging. *Stroke*. 2000;31(9):2175-2181. [CrossRef]
7. Minnerup J, Wersching H, Ringelstein EB, et al. Prediction of malignant middle cerebral artery infarction using computed tomography-based intracranial volume reserve measurements. *Stroke*. 2011;42(12):3403-3409. [CrossRef]
8. Kürten S, Munoz C, Beseoglu K, et al. Decompressive hemicraniectomy for malignant middle cerebral artery infarction including patients with additional involvement of the anterior and/or posterior cerebral artery territory-outcome analysis and definition of prognostic factors. *Acta Neurochir (Wien)*. 2018;160(1):83-89. [CrossRef]
9. Sikiö M, Kölhi P, Ryymin P, et al. MRI texture analysis and diffusion tensor imaging in chronic right hemisphere ischemic stroke. *J Neuroimaging*. 2015;25(4):614-619. [CrossRef]
10. Kauw F, Bennink E, de Jong HWAM, et al. DUST Investigators; DUST (Dutch Acute Stroke Study) investigators are as follows. Intracranial cerebrospinal fluid volume as a predictor of malignant middle cerebral artery infarction. *Stroke*. 2019;50(6):STROKEAHA119024882. [CrossRef]
11. Walcott BP, Miller JC, Kwon CS, et al. Outcomes in severe middle cerebral artery ischemic stroke. *Neurocrit Care*. 2014;21(1):20-26. [CrossRef]
12. Du M, Huang X, Li S, et al. A nomogram model to predict malignant cerebral edema in ischemic stroke patients treated with endovascular thrombectomy: an observational study. *Neuropsychiatr Dis Treat*. 2020;16:2913-2920. [CrossRef]
13. Mokin M, Primiani CT, Siddiqui AH, Turk AS. ASPECTS (Alberta Stroke Program Early CT Score) measurement using hounsfield unit values when selecting patients for stroke thrombectomy. *Stroke*. 2017;48(6):1574-1579. [CrossRef]
14. Puetz V, Dzialowski I, Hill MD, et al. Intracranial thrombus extent predicts clinical outcome, final infarct size and hemorrhagic transformation in ischemic stroke: the clot burden score. *Int J Stroke*. 2008;3(4):230-236. [CrossRef]
15. Tan IY, Demchuk AM, Hopyan J, et al. CT angiography clot burden score and collateral score: correlation with clinical and radiologic outcomes in acute middle cerebral artery infarct. *AJNR Am J Neuroradiol*. 2009;30(3):525-531. [CrossRef]
16. DeLong ER, DeLong DM, Clarke-Pearson DL. Comparing the areas under two or more correlated receiver operating characteristic curves: a nonparametric approach. *Biometrics*. 1988;44(3):837-845. [CrossRef]
17. Shu Z, Fang S, Ding Z, et al. MRI-based radiomics nomogram to detect primary rectal cancer with synchronous liver metastases. *Sci Rep*. 2019;9(1):3374. [CrossRef]
18. Vassileva E, Stoyanov P, Vavrek E, Stamenova P. Unexpected arterial recanalization after decompressive hemicraniectomy. *J Stroke Cerebrovasc Dis*. 2013;22(8):e661-3. [CrossRef]
19. Bosche B, Dohmen C, Graf R, et al. Extracellular concentrations of non-transmitter amino acids in peri-infarct tissue of patients predict malignant middle cerebral artery infarction. *Stroke*. 2003;34(12):2908-2913. [CrossRef]
20. Dohmen C, Bosche B, Graf R, et al. Identification and clinical impact of impaired cerebrovascular autoregulation in patients with malignant middle cerebral artery infarction. *Stroke*. 2007;38(1):56-61. [CrossRef]
21. Thomalla G, Hartmann F, Juettler E, et al. Clinical Trial Net of the German Competence Network Stroke. Prediction of malignant middle cerebral artery infarction by magnetic resonance imaging within 6 hours of symptom onset: A prospective multicenter observational study. *Ann Neurol*. 2010;68(4):435-445. [CrossRef]
22. Cho DY, Chen TC, Lee HC. Ultra-early decompressive craniectomy for malignant middle cerebral artery infarction. *Surg Neurol*. 2003;60(3):227-32; discussion 232-233. [CrossRef]
23. Castellano G, Bonilha L, Li LM, Cendes F. Texture analysis of medical images. *Clin Radiol*. 2004;59(12):1061-1069. [CrossRef]
24. Peter R, Korfiatis P, Blezek D, et al. A quantitative symmetry-based analysis of hyperacute ischemic stroke lesions in noncontrast computed tomography. *Med Phys*. 2017;44:192-199. [CrossRef]
25. Oliveira MS, Fernandes PT, Avelar WM, et al. Texture analysis of computed tomography images of acute ischemic stroke patients. *Braz J Med Biol Res*. 2009;42(11):1076-1079. [CrossRef]
26. Yao X, Mao L, Lv S, et al. CT radiomics features as a diagnostic tool for classifying basal ganglia infarction onset time. *J Neurol Sci*. 2020;412:116730. [CrossRef]
27. Kuang H, Najm M, Chakraborty D, et al. Automated ASPECTS on noncontrast CT scans in patients with acute ischemic stroke using machine learning. *AJNR Am J Neuroradiol*. 2019;40(1):33-38. [CrossRef]
28. Ortiz-Ramón R, Valdés Hernández MDC, González-Castro V, et al. Identification of the presence of ischaemic stroke lesions by means of texture analysis on brain magnetic resonance images. *Comput Med Imaging Graph*. 2019;74:12-24. [CrossRef]
29. Kassner A, Liu F, Thornhill RE, Tomlinson G, Mikulis DJ. Prediction of hemorrhagic transformation in acute ischemic stroke using texture analysis of postcontrast T1-weighted MR images. *J Magn Reson Imaging*. 2009;30(5):933-941. [CrossRef]
30. Betrouni N, Yasmina M, Bombois S, et al. Texture features of magnetic resonance images: an early marker of post-stroke cognitive impairment. *Transl Stroke Res*. 2020;11(4):643-652. [CrossRef]
31. Tracol C, Vannier S, Hurel C, et al. Predictors of malignant middle cerebral artery infarction after mechanical thrombectomy. *Rev Neurol (Paris)*. 2020;176(7-8):619-625. [CrossRef]
32. Park J, Goh DH, Sung JK, et al. Timely assessment of infarct volume and brain atrophy in acute hemispheric infarction for early surgical decompression: strict cutoff criteria with high specificity. *Acta Neurochir (Wien)*. 2012;154(1):79-85. [CrossRef]
33. Fuhrer H, Schönenberger S, Niesen WD, et al. Endovascular stroke treatment's impact on malignant type of edema (ESTIMATE). *J Neurol*. 2019;266(1):223-231. [CrossRef]
34. Birkhahn M, Mitra AP, Cote RJ. Molecular markers for bladder cancer: the road to a multimarker approach. *Expert Rev Anticancer Ther*. 2007;7(12):1717-1727. [CrossRef]

Supplementary Materials

Least absolute shrinkage and selection operator (LASSO) is a powerful algorithm for regression analysis with high dimensional predictors. In our study, we used LASSO to select the most important predictive features in the training set based on the "glmnet" package in R statistical software version 3.3.1. There were 15 most valuable radiomics features left following LASSO. Details of the 15 radiomics features are shown in Supplementary Table 1. The multivariate logistic regression was used to build the model of LASSO. At last, a formula was generated using a linear combination of selected features that were weighted by their respective LASSO coefficients.

Supplementary Table 1. Information of radiomics features selected by least absolute shrinkage and selection operator

Category	Feature	Description
RLM	HighGreyLevelRunEmphasis_AllDirection_offset1_SD LongRunEmphasis_angle0_offset4 LongRunHighGreyLevelEmphasis_AllDirection_offset4_SD LongRunLowGreyLevelEmphasis_angle45_offset4 ShortRunEmphasis_angle45_offset7	The grey level run-length matrix (RLM) is defined as the numbers of runs with pixels of gray level *i* and run length *j* for a given direction θ. RLMs is generated for each sample image segment having directions (0°,45°,90° &135°).
GLCM	Inertia_AllDirection_offset4_SD differenceVariance sumEntropy	The grey level co-occurrence matrix (GLCM) represents the joint probability of certain sets of pixels having certain grey-level values. It calculates how many times a pixel with grey-level *i* occurs jointly with another pixel having a grey value *j*, by varying the displacement vector d between each pair of pixels.
Histogram	MinIntensity Percentile10 VoxelValueSum ClusterShade_AllDirection_offset7_SD	Histogram parameters are concerned with properties of individual pixels. They describe the distribution of voxel intensities within the computed tomography image through commonly used and basic metrics.
Form factor	Compactness2 Sphericity	Form factor parameters include descriptors of the three-dimensional size and shape of the lesion region.
GLSZM	HighIntensitySmallAreaEmphasis	The gray level size zone matrix (GLSZM) is the starting point of Thibault matrices. For a texture image f with N gray levels, it is denoted GSf(s, g) and provides a statistical representation by the estimation of a bivariate conditional probability density function of the image distribution values. It is calculated according to the pioneering Run Length Matrix principle: the value of the matrix GSf (s, g) is equal to the number of zones of size s and of gray level g. The resulting matrix has a fixed number of lines equal to N, the number of gray levels, and a dynamic number of columns, determined by the size of the largest zone as well as the size quantization.

Rad-score calculation formula

Rad-score = -0.8398+0.8269×MinIntensity
-0.5822× Percentile10
-0.3390×VoxelValueSum
-0.5025×ClusterShade_AllDirection_offset7_SD
-1.6389×Inertia_AllDirection_offset4_SD
+0.7927×differenceVariance
+0.2364×sumEntropy
+0.0480×HighGreyLevelRunEmphasis_AllDirection_offset1_SD
+0.0517×LongRunEmphasis_angle0_offset4
+0.2528×LongRunHighGreyLevelEmphasis_AllDirection_offset4_SD
+7.4376×LongRunLowGreyLevelEmphasis_angle45_offset4
-0.3203×ShortRunEmphasis_angle45_offset7
+0.4199×Compactness2
-0.2494×Sphericity
-0.7987×HighIntensitySmallAreaEmphasis